ASTM INTERNATIONAL

Geotechnical Testing Journal

D. E. Escribano,[1] D. F. T. Nash,[2] and A. Diambra[2]

DOI: 10.1520/GTJ20170054

Local and Global Volumetric Strain Comparison in Sand Specimens Subjected to Drained Cyclic and Monotonic Triaxial Compression Loading

Geotechnical Testing Journal

doi:10.1520/GTJ20170054 available online at www.astm.org

D. E. Escribano,[1] D. F. T. Nash,[2] and A. Diambra[2]

Local and Global Volumetric Strain Comparison in Sand Specimens Subjected to Drained Cyclic and Monotonic Triaxial Compression Loading

Reference

Escribano, D. E., Nash, D. F. T., and Diambra, A., "Local and Global Volumetric Strain Comparison in Sand Specimens Subjected to Drained Cyclic and Monotonic Triaxial Compression Loading," *Geotechnical Testing Journal* https://doi.org/10.1520/GTJ20170054. ISSN 0149-6115

ABSTRACT

This article investigates the development of volumetric strain nonuniformities in sand specimens subjected to drained cyclic triaxial compression loading. The assessment is performed by comparing volumetric strain determinations using an external volume gauge and local axial and radial strain measurements mounted on the center of the specimen. The experimental investigation has been performed for both frictional and enlarged lubricated ends on sand specimens of different densities and fabricated using both moist tamping and dry deposition techniques. It will be shown that considerable discrepancies between the global and local volumetric determination arise even in specimens tested with enlarged lubricated ends, as a result of different volumetric tendencies (contraction or dilation) of the center and the boundaries of the specimens. These discrepancies are more pronounced for dense specimens cycled at high average stress ratios and amplitudes. The influence of three different assumptions employed to account for the specimen's deformed profile (namely the right cylinder, parabolic, and sinusoidal profile) on the local volumetric determinations will be also assessed. Some recommendations for the need for local volumetric measurements will be attempted.

Keywords

sand, strains, triaxial testing, end restraint, cyclic loading

Manuscript received February 21, 2017; accepted for publication April 26, 2018; published online September 20, 2018.

[1] Department of Civil Engineering, University of Concepción, Chile (Corresponding author), e-mail: describano@udec.cl, https://orcid.org/0000-0003-2014-9008

[2] Department of Civil Engineering, University of Bristol, Queen's Building, University Walk, Bristol BS4 3NJ, United Kingdom (D.F.T.N. deceased)

Nomenclature

β = Cyclic stress amplitude ratio, equal to $\Delta q/p'$
C_u = Coefficient of uniformity
C_g = Coefficient of gradation
D_{10} = Soil particle diameter at which 10 % of the soil mass is finer
D_{30} = Soil particle diameter at which 30 % of the soil mass is finer
D_{60} = Soil particle diameter at which 60 % of the soil mass is finer
D_o = Initial diameter of the specimen
D_1 = Diameter of the specimen measured at mid-height with the radial transducer
ε_a = Axial strain
$\varepsilon_a(G)$ = Global axial strain
ε_v = Volumetric strain
ε_r = Radial strain
e = Void ratio
$e_{\min}$ = Minimum void ratio
$e_{\max}$ = Maximum void ratio
H = Height of specimen
L = Gauge length
η = Stress ratio equal to q/p'
N = Number of cycles
N_d = Number of cycles when global volumetric strains move from positive to negative values
M_c = Critical state stress ratio
p' = Mean effective stress
Δq = Peak to peak cyclic stress amplitude
q = Deviator stress
S_r = Slenderness ratio equal to H_o/D_o

Introduction

One of the major limitations of the triaxial apparatus is the restraint applied at the specimen ends. When conventional end platens are used, the friction between the specimen and the bottom and top caps restricts the specimen from deforming laterally, thereby inducing nonuniform stress distributions and deformations across the specimen, which may assume a "barrel shape" when undergoing compression. Testing specimens with slenderness ratio S_r (height to diameter ratio) between 1.5 and 3 is a common practice to minimize the end restraint effects on the middle third of the specimen (Bishop and Green 1965), where the deformations are expected to be more uniform and least affected by end restraints. The barreling can cause a large discrepancy between volume change measurements using global gauges and those deduced from local strain transducers, thus possibly leading to misinterpretation of the soil behavior (Linton, McVay, and Bloomquist 1988; Klotz and Coop 2002).

Enlarged lubricated ends (LE) are sometimes employed to minimize the friction at the boundaries (Rowe and Barden 1964; Kirkpatrick and Belshaw 1968), and even short specimens ($S_r = 1$) may experience a more homogeneous deformation pattern than conventional $S_r = 2$ specimens tested with frictional end platens (Goto and Tatsuoka 1988).

However, Linton, McVay, and Bloomquist (1988) and Klotz and Coop (2002) demonstrated that, despite the use of LE, specimens may still be subjected to some end restraint and may still develop strain nonuniformities, which in turn affect both the local and global determinations of the specimen's volumetric behavior. Recent experiments using digital image processing methods (Liu, Longtan, and Xiaoxia 2013) confirmed that deformations in a triaxial soil specimen were more uniform in the middle region when compared to the entire specimen, and that using measurements from this region was more effective in eliminating the effects of end restraint than the use of LE platens.

The intepretation of the volumetric behavior from local measurements should also take the deformed shape of the specimens into account. If the specimen assumes a barrel shape, the radial strain measurements at the mid-height of the specimen exceed the average value, and if the barreling is too great, the axial transducers may be pushed out of aligment and give false readings. Thus, different deformation assumptions rather than the conventional right cylinder (RC) have been employed in the literature, even when LE platens were employed. Germaine and Ladd (1988) and Zhang and Garga (1997) found that the maximum diameter of a triaxial sand specimen occurred at mid-height, and it changed with the height following a parabolic shape. Klotz and Coop (2002) assumed that the sides of the specimen were deforming as an arc, and no lateral deformations were developed at the ends of the specimen.

The development of nonuniformities in strain and stress distributions are also influenced by the specimen density and fabrication method. Vardoulakis and Drescher (1985) demonstrated that dense specimens exhibit more prounounced nonuniformities and strain localization when compared to looser specimens. Before localization develops, the specimen may bulge and present other bifurcation deformation modes, whose onset can be delayed by the presence of LE platens and a uniform method of specimen preparation (Desrues 1990; Desrues, Bésuelle, and Lewis 2007). Depending on the fabrication method of the specimen, nonunformities of density across the specimen may be present and thus affect the uniformity of deformation during loading.

While the achievement of precise and accurate measurement of specimen deformations and the proper account of nonuniformities and localization issues are still ongoing research topics, most of the previous experimental work has concentrated on the monotonic shearing behavior of soils (Desrues 1984; Colliat-Dangus, Desrues, and Foray 1988). The research reported here aimed to expand the current state of the knowledge by exploring the development of nonuniformities in sand specimens subjected to up to 4,000 drained compressive load cycles in the triaxial apparatus, as part of experimental and constitutive modeling research at the University of Bristol, United Kingdom (Corti et al. 2016). The nonuniformity of deformations across the specimen has been examined by comparing volume changes using both global and local measurements. Three different deformed shapes for the specimens have been considered, and the sensitivity of the interpretation of experimental results to these assumptions has been investigated. The influence on the nonuniformities to (i) the end boundary conditions (frictional and enlarged LE), (ii) specimen density, and (iii) specimen fabrication method (moist tamping, MT, and dry deposition, DD) will be discussed.

Models for Calculation of Volumetric Strains

A schematic representation of a soil specimen instrumented with local axial and radial strain transducers and deformed during triaxial compression is shown in **Fig. 1**. The

FIG. 1

Assumed conditions of the triaxial specimen for barreling correction.

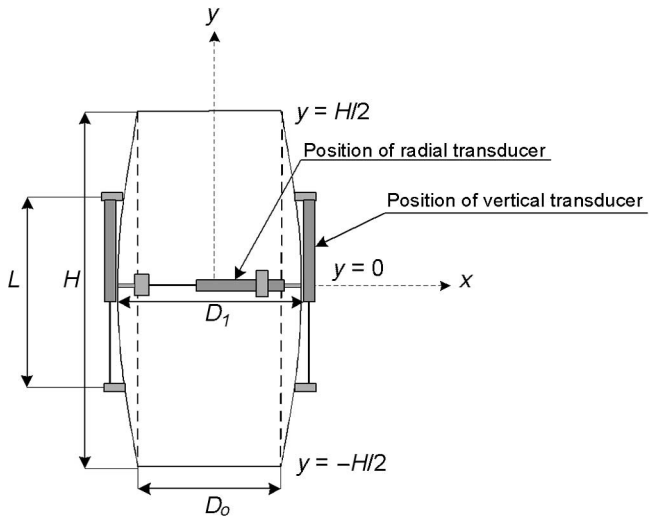

geometry of a specimen of current height H is described using an x–y coordinate system whose origin is located at the center of the specimen. The gauge length of the local axial transducers (LVDT) is defined by L, which varied between 50 to 52 mm in the present experimental work and spanned the specimen at mid-height to monitor the behavior in its central third. The diameter D of the specimen varies with height; during a compression test, the diameter is generally largest at mid-height (D_1) and decreases toward the specimen ends (D_o).

In order to calculate volumetric strains from the measured values of local axial and radial strains, three different assumptions for the deformed shape of the specimen have been considered: RC, parabolic shape, and sinusoidal shape, which are shown in Fig. 2a–c, respectively. It is emphasized that the following expressions for estimation of the volumetric strain refer to the instrumented central portion of the specimen. Compressive strains are assumed positive in this work.

FIG. 2

Assumed deformation models for triaxial specimens subjected to compression. (a) Right cylinder, (b) parabolic profile, and (c) sinusoidal profile.

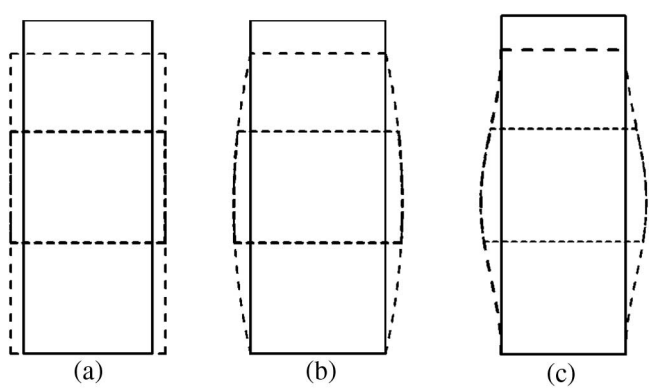

RC

The RC assumption considers that lateral deformations are homogeneous through the height of the specimen (see Fig. 2a), with the specimen's diameter constant and equal to the value measured by the radial strain transducer located at mid-height. For this case, the volumetric strain ε_v of the specimen can be determined from the measured local radial and axial strains, ε_r and ε_a respectively, using the following second order expression:

$$\varepsilon_v = \varepsilon_a + 2\varepsilon_r - 2\varepsilon_a\varepsilon_r - \varepsilon_r^2 + \varepsilon_r^2\varepsilon_a \tag{1}$$

PARABOLIC SHAPE

The assumption of a parabolic specimen profile follows the proposal by Germaine and Ladd (1988) and Zhang and Garga (1997) from the experimental observation of triaxial specimens sheared in compression. With this assumption, the variation of the diameter D along the specimen height can be described with the following expression:

$$D = D_1 - (D_1 - D_o) \cdot \left(\frac{2y}{H}\right)^2 \tag{2}$$

Where D_1 is the maximum specimen diameter located at mid-height (y = 0), and D_o is the diameter at its ends (y = ±H/2), which is equal to the initial specimen diameter under the assumption of no lateral deformation at the specimen-cap interface (Klotz and Coop 2002). By the integration of Eq 2 over the instrumented section of the specimen it is possible to obtain (see Appendix) the following expression for the volumetric strain from the measured local axial and radial strains:

$$\varepsilon_v = \left[2 \cdot \left(1 - \frac{1}{3}\left(\frac{L}{H}\right)^2\right) \cdot \varepsilon_r + \left(-1 + \frac{2}{3} \cdot \left(\frac{L}{H}\right)^2 - \frac{1}{5} \cdot \left(\frac{L}{H}\right)^4\right) \cdot \varepsilon_r^2\right] \cdot (1 - \varepsilon_a) + \varepsilon_a \tag{3}$$

It should be noted that the height (H) and length (L) of the instrumented central portion of the specimen change during the test, but their ratio is assumed to stay constant.

SINUSOIDAL

An alternative assumption, which assumes that the specimen's diameter follows a cosinusoidal variation with the specimen height, is considered (see Fig. 2c). Unlike the parabolic shape, this expression implies that the tangent of the specimen profile is vertical at the ends of the specimen. Thus, the effect of a different assumption for the deformed shape on the interpretation of volumetric deformations may be examined. The variation of diameter D with the height of the specimen is expressed by the following:

$$D = D_o - \frac{(D_1 - D_o)}{2}\left[1 + \cos\left(\pi \cdot \frac{2y}{H}\right)\right] \tag{4}$$

In a similar manner (see Appendix), the integration of Eq 4 leads to the following expression of the volumetric strains on the instrumented central part of the specimen:

$$\varepsilon_v = \left[\left(1 + \frac{H}{\pi \cdot L}\sin\left(\pi \cdot \frac{L}{H}\right)\right) \cdot \varepsilon_r + \left(-\frac{3}{8} - \frac{\sin(\pi \cdot L/H)}{2\pi \cdot L/H} - \frac{\sin(2\pi \cdot L/H)}{16\pi \cdot L/H}\right) \cdot \varepsilon_r^2\right] \cdot (1 - \varepsilon_a) + \varepsilon_a \tag{5}$$

Materials

Triaxial experimental tests were conducted on Hostun S28 sand, which is a subangular granular siliceous medium material that has been widely used in the past for experimental research and constitutive modeling (Sadek 2006; Doanh and Ibraim 2000; Diambra et al. 2011). A typical particle size distribution of this sand is given in **Fig. 3**, and it is characterized by a mean grain size $D_{50} = 0.35$ mm, coefficient of uniformity $C_u = D_{60}/D_{10} = 1.59$, coefficient of curvature $C_g = (D_{30})^2/(D_{10}D_{60}) = 0.97$, maximum and minimum void ratio $e_{max} = 1.00$ and $e_{min} = 0.656$, and specific gravity $G_s = 2.65$ (Escribano 2014), which were determined following BS EN ISO 17892, *Geotechnical Investigation and Testing. Laboratory Testing of Soil. Determination of Particle Density*. Further information on other properties of this Hostun RF sand can be found in Flavigny, Desrues, and Palayer (1990).

Specimen Preparation

The specimens were tested using two different boundary conditions in order to study their influence on the development of nonuniformities and volumetric deformations during drained cyclic loading: (i) fully frictional end platens and (ii) enlarged LE platens. In this investigation, two different specimen preparation methods were also used: (i) MT with under-compaction (Ladd 1978) and (ii) the DD method (Ishihara 1993). The details of each are described in the following paragraphs.

SPECIMEN BOUNDARY CONDITIONS

Specimens with fully frictional ends (defined here as restrained ends, RE) had a height to diameter ratio $S_r = 2$, a diameter of 75 mm, and a height of 150 mm. Specimens with enlarged LE had dimensions of 140-mm height and 70-mm diameter with one drainage line at the center. The LE consisted of smooth silicone grease and three layers of latex rubber discs (0.3-mm thickness) with several radial cuts to minimize their resistance to radial stretching.

FIG. 3

Grain size distribution of Hostun sand.

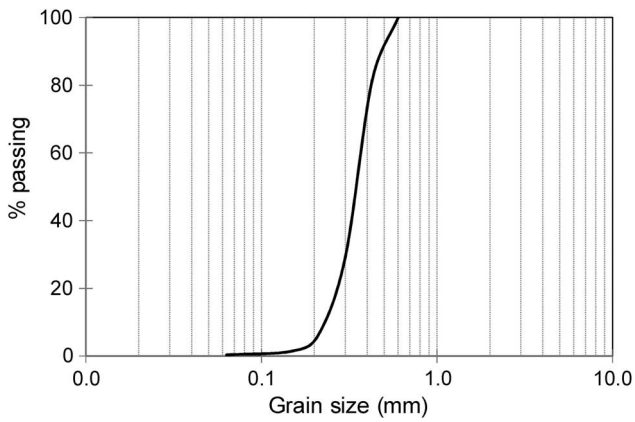

SPECIMEN FABRICATION

Moist Tamping Technique

In preparing specimens using the MT method with under-compaction (Ladd 1978), the total amount of dry soil required was mixed with a predetermined amount of water and divided into several equal parts. The value of 10 % moisture content, used for the dense specimens, corresponded to the optimum value obtained from compaction tests (Ibraim and Fourmont 2006), while the use of lower water contents simplified the fabrication of looser specimens. The specimens were then prepared in layers, each tamped to a certain predetermined height with the purpose of controlling its density and avoiding over-compaction of the layers underneath. Each specimen was formed from 10 layers, giving a layer thickness of 15 mm for a specimen of 150-mm height and 14 mm for specimens of 140-mm height.

Dry Deposition Technique

In this procedure, a predetermined amount of dry sand was carefully poured inside a mold using a funnel, ensuring a zero height of fall and uniformly spreading the sand across the specimen. The target density was then reached by tapping the sides of the mold with a gentle vibrator. Any nonuniformity on the final specimen's top surface was leveled off with a brush, and the top cap was subsequently installed. Particular care was paid in order to minimize the creation of looser zones as a result of the brushing.

Experimental Equipment and Procedures

EXPERIMENTAL EQUIPMENT

Drained cyclic triaxial tests were performed using an hydraulic stress path triaxial apparatus (Bishop and Wesley 1975) equipped with an internal load cell with an accuracy of ±1.5 N, differential pressure transducer with ±0.7 kPa of accuracy, external LVDT with an accuracy of ±0.02 % of strain, and Imperial College type volume gauge (±0.05 milliliters of accuracy).

LOCAL STRAIN TRANSDUCERS

Three local miniature submersible LVDTs (RDP D5W, RDP Electrosense, Pottstown, PA) similar to the ones described by Cuccovillo and Coop (1997), with a 5 mm displacement range, output voltage level of ±10 V, and accuracy of ±0.005 % of strain, were used to measure axial and radial strains in the middle third of the specimens. As shown in **Fig. 1**, two vertical transducers were mounted opposite each other, each fixed to an upper pad with its armature resting on a lower pad. The average results of the two LVDTs were used to calculate axial strain. A third transducer was mounted horizontally on a radial belt installed at the middle of the specimen. To ensure alignment between the upper and lower pads of the axial gauges, small aluminum arms were temporarily located between the top and bottom pads. The pads were then glued on the sides of the specimen with instant contact adhesive and pins protruded into the specimen. A similar connection was used for the radial belt. A fixed connection between the load cell and top cap helped to avoid misalignment errors and therefore minimized the difference in readings between the two opposite axial LVDTs. A photograph of a fully instrumented specimen with enlarged LE is provided in **Fig. 4**.

LVDTs can be highly affected by temperature fluctuations of the water in the cell. Even a 1°C variation of the water temperature produces significant oscillations on the

FIG. 4

Triaxial specimen instrumented by vertical and radial LVDTs.

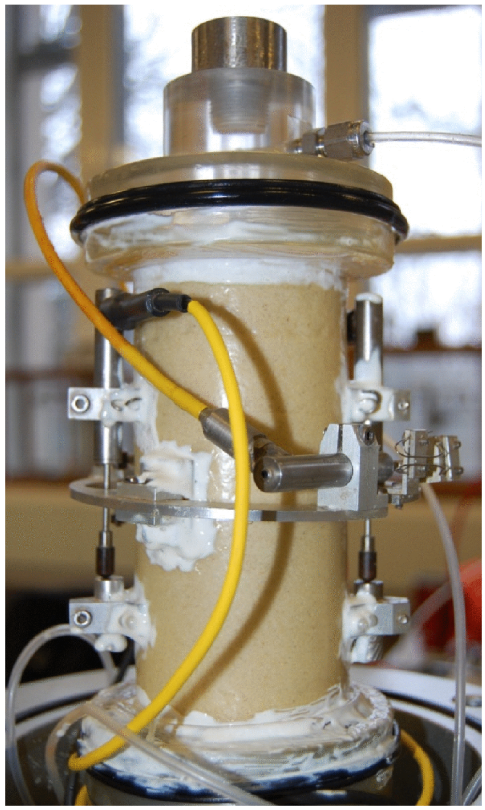

LVDT readings. The room temperature was controlled, and the triaxial cell was covered with bubble wrap, which generally decreased the temperature changes to 0.2°C.

TRIAXIAL TEST CONDITIONS

After its preparation, the initial dimensions of the specimen were taken while applying 25 kPa of vacuum. Fully saturated specimens were then produced by initially circulating carbon dioxide for 1 hour at a differential pressure of 3 kPa; then deaired water was circulated from the bottom to the top of the specimen. Finally, the back pressure was raised to between 200 and 400 kPa until a Skempton B value higher than 0.95 was obtained. Changes in the specimen's height and diameter during saturation were monitored through the internal vertical and radial transducers. These measurements have been used to correct the specimen's initial void ratio.

A schematic representation of the stress path followed during the tests is shown in Fig. 5 in terms of stress ratio $\eta = q/p'$ (ratio between the deviator stress q and the mean effective stress p') versus the mean isotropic stress p'. Isotropic consolidation to a target value of mean effective stress of p'_0 was achieved by increasing the cell pressure at a rate of 60 kPa per hour. Any further anisotropic consolidation to reach a desired average stress ratio η_{avg} was then undertaken, maintaining the mean effective stress constant. At the end of consolidation, creep under constant stress conditions was allowed for a maximum of two hours before the start of cyclic loading. In most tests, cyclic loading was applied

FIG. 5

Schematic representation of the stress paths imposed during experimental tests listed in Table 1.

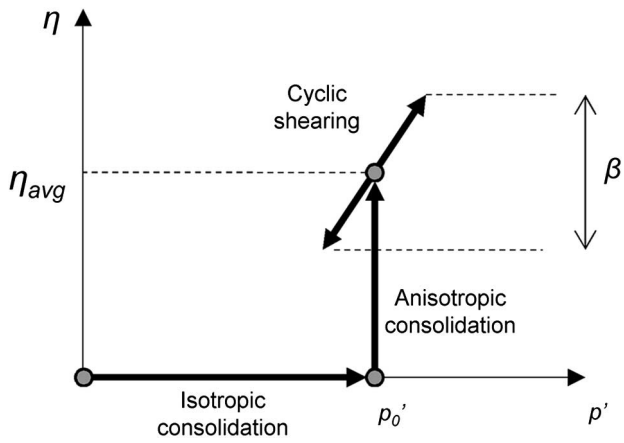

around the average stress ratio η_{avg} by varying the axial stress sinusoidally with time, keeping the cell pressure constant. A low frequency of 1 cycle per 5 minutes was applied in order to ensure well-defined cycles and homogeneous pore water pressure inside the specimen.

The amplitude of the cyclic stress ratio is described using $\beta = \Delta q/p_0$', defined as the ratio of peak to peak cyclic stress amplitude Δq to the average mean effective stress p'_0 (see Fig. 5). Tests were performed at different stress levels, cyclic stress amplitudes, and initial densities. Most tests were one of the following types: stresses cycled only in compression (i) at low η_{avg} and (ii) at high η_{avg} and (iii) stresses cycled from compression to extension and (iv) stresses cycled only in extension at low η_{avg}. One test (DDLE_5) utilized several stages of cyclic loading carried out when monotonic loading in compression was interrupted; each stage had a small number of cycles in which the deviatoric stresses were decreased from the current maximum value reached.

Table 1 summarizes the tests performed in this campaign, providing details on the fabrication method and testing conditions. It is possible to divide the test program into three groups characterized by different specimen preparation methods (MT or DD) and employed boundary conditions (RE, LE); hence, tests are classified as MTRE, MTLE, and DDLE in Table 1 for a total of 16 tests. Table 1 also specifies which specimens have been monotonically sheared in drained conditions after the cyclic loading state: some specimens were sheared at constant mean effective stress p', while others were sheared at constant cell pressure. The final monotonic shearing was continued until the local strain transducers reached their working limit.

Comparisons between Global and Local Strain Measurements

Differences between global axial strains measured externally and local axial strains measured with transducers mounted on the specimen are commonly observed in monotonic tests and are due to bedding errors and nonuniformities developed during the test. The external measurement of volume change may be used to determine the average volumetric

TABLE 1
List of tests performed.

Test Number	e	p_0', kPa	Dr, %	η_{avg}	β	N	Monotonic Loading	Specimen Prep. Method	End Conditions
MTRE_1	0.966	100	9.88	0.10	0.32–1.4	3,500[a]	const σ'_3	MT	RE
MTRE_2	0.977	100	6.69	0.25	0.31–0.59	1,000	const σ'_3	MT	RE
MTRE_3	0.740	100	75.13	0.25	0.33	1,500	–	MT	RE
MTRE_4	0.899	100	29.36	0.50	0.31–0.92	250	const p'	MT	RE
MTRE_5	0.727	100	79.36	1.00	0.35	1,000	const p'	MT	RE
MTRE_6	0.74	100	75.59	−0.30	0.40	4,000	ext const σ'_3	MT	RE
MTLE_1	0.937	100	18.31	0.50	0.36	1,500	const σ'_3	MT	LE
MTLE_2	0.720	100	81.85	0.50	0.34	1,500	–	MT	LE
MTLE_3	0.982	100	5.23	1.00	0.39	350	–	MT	LE
MTLE_4	0.722	100	80.81	1.00	0.34	1,500	const σ'_3	MT	LE
MTLE_5	0.717	100	82.27	1.28	0.34	1,500	const σ'_3	MT	LE
DDLE_1	0.984	50	4.65	0.00	0.35	250[a]	–	DD	LE
DDLE_2	0.985	100	4.36	0.25	0.34	250	const p'	DD	LE
DDLE_3	0.913	75	25.29	0.50	0.47	200	const p'	DD	LE
DDLE_4	0.796	100	59.30	0.50	0.47	200	const σ'_3	DD	LE
DDLE_5	0.824	100	51.16	0.20–1.40	0.18–1.21	5-50	const p'	DD	LE

Note: [a] Denotes two-way cycling where $\beta/2 > \eta_{avg}$.

strain and hence, using the RC assumption, the average radial strain. Such measurements are susceptible to errors arising from leakage and temperature change, although in this research attempts were made to minimize these. The direct measurement of radial movements permits the determination of radial strain at mid-height of the specimen, and when combined with the local axial strain measurements and an assumption about the specimen shape, the volumetric strains in the instrumented section may be determined.

Examples of the measurements undertaken are shown in Fig. 6a–d for the compression test MTRE_5 and the extension test MTRE_6, both on dense specimens prepared by MT with RE. Each specimen was cycled around an average stress ratio before the deviatoric stresses were increased. Fig. 6a shows plots of the stress ratio q/p' versus global and local axial, radial, and volumetric strains. The local volumetric strains were determined using the sinusoidal shape of the specimen deformed profile. Fig. 6b reports the trends of global and local volume strains (determined with Eqs 1, 3, and 5 for the RC, parabolic (P) and sinusoidal (S) deformed shape, respectively, and also imposing null radial strains ($\varepsilon_r = 0$)) versus local axial strain. Several observations can be made:

1. Global axial strains exceed the local axial strains significantly in both cases;
2. During cyclic loading in compression (see Fig. 6a), the volume changes measured locally are very small, primarily because the radial strains are extremely small;
3. During cyclic loading at low stress ratios in extension (see Fig. 6c), the volume changes measured locally are also small, although the radial strains are slightly larger; and
4. At large strains the magnitude and rate of dilation are smaller using the external measurements than those calculated from the local measurements.

Fig. 6e and f show similar plots for test MTRE_1, a loose specimen that was subjected to two-way symmetric cycling before being tested to failure in compression. In this test, the strains developed during cycling were larger than those in the previous tests. After cycling,

FIG. 6 (a,b) Compression test MTRE_5, (c,d) extension test MTRE_6, and (e,f) two-way cycled test MTRE_1 showing variations of q/p' versus global and local strains and global and local volumetric strains versus local axial strains, respectively.

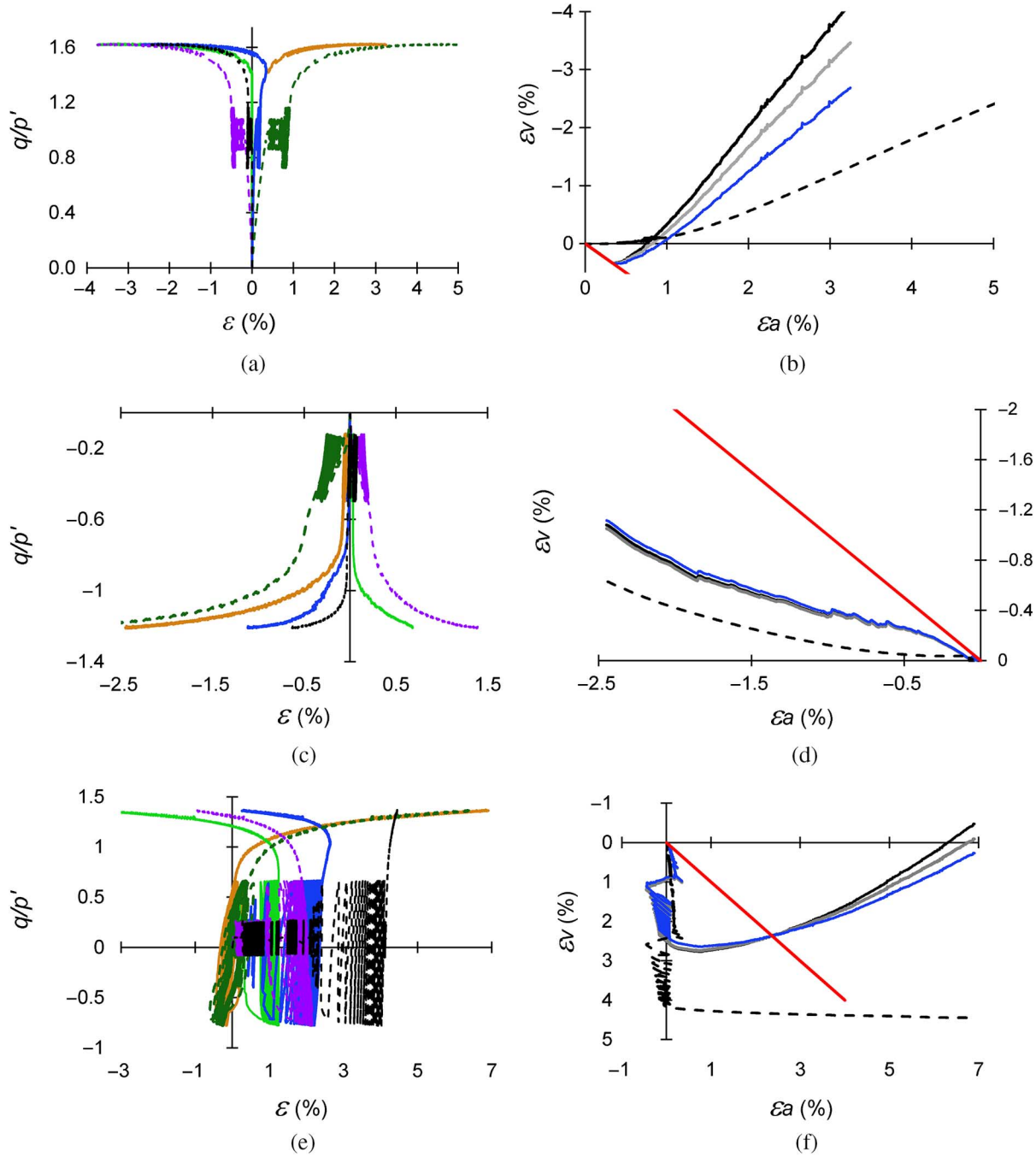

the axial strains were small, but the specimen showed significant volumetric contraction; the volumetric strain measured externally was twice that deduced from the local measurements.

In the following sections, the global and local strains from a number of tests are compared both at large strains and in the small strain range. In some tests, there were indications that temperature fluctuations were unduly influencing the external volume measurements, or that the radial displacement transducer was sticking; these tests have been excluded from the comparisons.

BEHAVIOR AT LARGE STRAINS

Axial Strain Measurements

Fig. 7a–c show the comparison between local ε_a and global $\varepsilon_a(G)$ axial strains for all the compression tests that were loaded monotonically to large strains after experiencing cyclic loading. At large strains, there are some slight differences between the axial strains observed in tests with RE (MTRE) and some of those with LE (MTLE and DDLE). MTRE tests continue through the 1:1 line; instead, MTLE tests present larger global axial strains. On the other hand, DDLE tests for 25.3 % and 59.3 % relative density follow the 1:1 line, but the loose specimen, at 4.4 % relative density, presents larger global axial strains, as in the case of MTLE tests. This is probably related to inevitable bedding errors related to soft inclusions. However, despite some initial differences, the local and global strain rates at large strain are similar (i.e., the trends are rather parallel to the 1:1 line) in most of the tests.

Only one extension test is reported here (MTRE6), but Fig. 7d shows that the differences are particularly marked. In the small strain range (<0.5 %) the externally measured axial strains were more than 10 times those observed in the central part of the specimen, possibly produced because of initial friction in the LVDTs' armature due to misalignment. At large strains, the local axial strain rates were initially rather similar

FIG. 7 Comparison of local ε_a and global axial strain $\varepsilon_a(G)$ measurements for tests loaded monotonically to large strains: (a) MTRE tests, (b) MTLE tests, (c) DDLE tests, and (d) extension test.

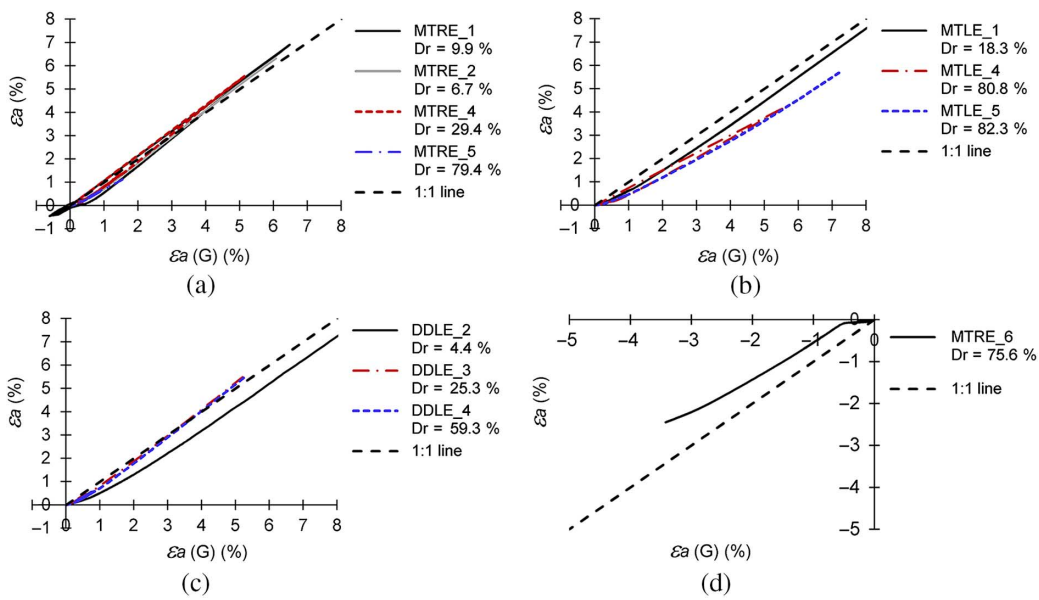

to the global strain rate, but then the global strain rate seems to progressively exceed that measured locally.

Volumetric Strains

For each set of compression tests shown in Table 1 (MTRE, MTLE, and DDLE groups), two specimens (one in a loose initial state and another in a medium dense to dense initial state) have been selected to illustrate the typical differences between the volumetric strains measured using the external volume gauge and that were calculated using the internal LVDTs. The three assumptions for specimen deformation previously introduced in the "Models for Calculation of Volumetric Strains" section (RC, parabolic, and sinusoidal deformation shapes) have been considered for the volumetric strains' determination using locally installed transducers.

The axial strain–volumetric strain trends for the six selected specimens are given in Fig. 8. The dotted red line included in the graphs corresponds to a 1:1 relationship between strains, to differentiate between expansion at mid-height (data above the 1:1 line) and contraction (data below the 1:1 line). For these tests loaded in compression, all the data lie above the 1:1 line, meaning that the soil is being deformed, as shown in Fig. 2. The initial section of the curves at small strains corresponds to the cyclic loading stage, and all the local strains lie on or very close to the 1:1 line, indicating that the radial strains are very small or negligible; as a result, the volumetric strains are initially of similar magnitude to the axial strains.

As shearing progresses and the stress ratio q/p' exceeds about 1.0 (see Fig. 8), the specimens start to expand at mid-height (radial strains are negative), producing differences

FIG. 8 Volumetric strain–axial strain curves for tests sheared in compression: (a) MTRE_2, (b) MTLE_1, (c) DDLE_2, (d) MTRE_5, (e) MTLE_5, and (f) DDLE_4.

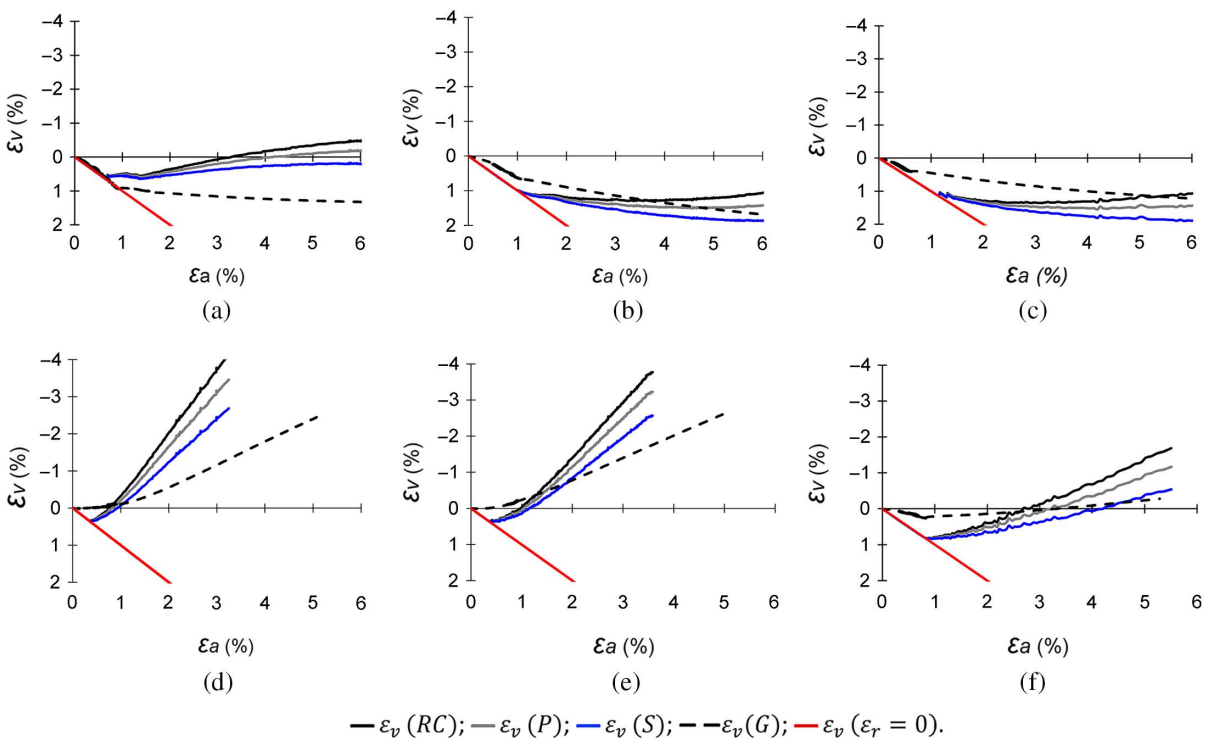

among the volumetric strains calculated with the three different deformation models shown in Fig. 2. The divergence between the three local strain determinations seems to occur with the onset of dilation, especially for the dense and medium dense specimens (Fig. 8d–f), and become significant above an axial strain level of 1 %, for both loose and dense specimens. By inspection of the radial strain measurements shown in Fig. 6, it can be determined that these differences arise when the radial strain exceeds approximately −0.25 %.

For the loose specimens, the average volumetric strain measured with the external volume gauge (global measurement) indicates continuous contraction as they are compressed (see Fig. 8a–c), while the local measurements show that an almost constant volume state is reached above 5 % axial strain. In the medium dense to dense specimens (see Fig. 8c–e) the global measurements indicate much smaller dilatancy rates than those calculated from the local measurements. In the single extension test reported here (see Fig. 6d), the dilatancy rate measured with local instrumentation was approximately twice that measured externally.

These differences are significant and suggest that local strain measurements are essential to interpret the state of the soil correctly. The selection of the most appropriate method for calculating the volumetric strain from the local measurements depends on the degree of end restraint and should be informed by observations of the actual shape after testing. Of the three methods, the RC assumption will always provide a limit, since the radial strain throughout the specimen is assumed constant and equal to that at mid-height. Visual observations of the specimens during and after testing suggested that the appropriate shape of deformation to consider when using local measurements on a triaxial specimen with $S_r = 2$ for monotonic loading is the sinusoidal assumption (see Fig. 2c). Fig. 8 also shows that there is no considerable difference in the predicted volumetric strains between the parabolic and sinusoidal assumptions, especially at the small strain level. Therefore, the sinusoidal shape assumption will be used to compare local and global strain measurements in the small strain range.

BEHAVIOR AT SMALL STRAINS UNDER CYCLIC LOADING

Accumulated Axial Strains

Since volumetric changes derive from both radial and axial deformations of the specimen, it seems appropriate to start the analysis with the comparison of accumulated axial strains measured by both local and external axial strain transducers ($\Delta\varepsilon_a$ and $\Delta\varepsilon_a(G)$, respectively) during the cyclic loading stage, defined as follows:

$$\Delta\varepsilon_a = \varepsilon_a - \varepsilon_{a_0} \quad \text{and} \quad \Delta\varepsilon_a(G) = \varepsilon_a(G) - \varepsilon_{a_0}(G) \tag{6}$$

Where ε_{a_0} and $\varepsilon_{a_0}(G)$ are the values of axial strain at the start of the first cycle measured with local and external transducers, respectively. Fig. 9 shows a comparison of the two determinations (local and external axial strains) for both fabrication procedures and boundary conditions employed. Except for tests in which loads cycled between compression and extension (MTRE 1 in Fig. 9a and DDLE 2 in Fig. 9c), the axial deformations developed during cyclic loading measured with the external transducer were significantly (up to five times) greater than those measured with the local transducers. The differences indicate that proportionately larger movements developed at the ends of the specimen throughout cyclic loading; a factor of five sounds large, but actually represents only about 0.25 mm of additional movement at each end.

FIG. 9 Comparison between global and local accumulated axial strains (%) during cyclic loading.

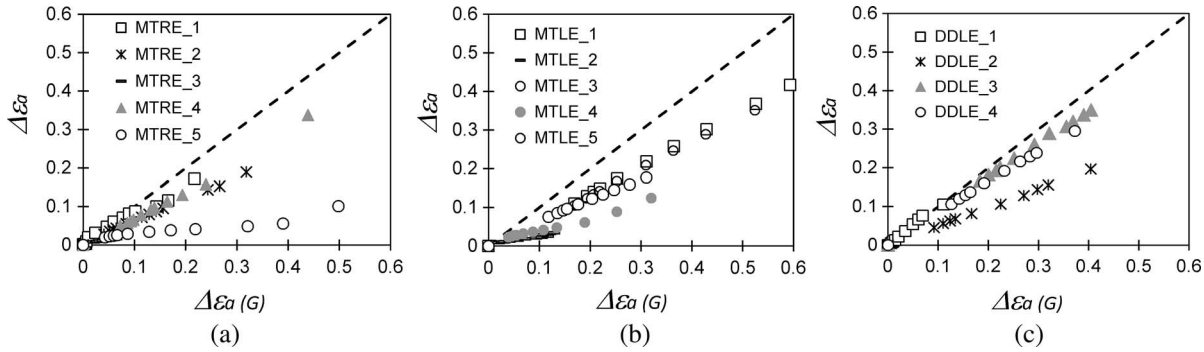

Accumulated Radial Strains

Direct measurements of the radial strains are only made locally but may be compared to radial strains calculated from the external volume and axial strain measurements. Fig. 6 showed that for test MTRE_5 cycled wholly in compression, the radial strains were very small. Fig. 10a shows the data from test MTRE_5 replotted for clarity, showing local and global radial strains plotted against each other and against *q/p'*. It can be seen that strains measured locally were extremely small during cycling and did not increase until the stress ratio *q/p'* reached about 1.4, at which point the specimen started to bulge and dilate; this contrasts with the strains calculated from the global measurements. During the subsequent monotonic loading, local and global radial strains became more similar at large strains.

Similar trends were observed in all specimens tested wholly in compression. The critical stress ratio at which radial strains started to increase has been plotted against relative density in Fig. 10b, its value increasing from about 0.8 for loose specimens to 1.4 for dense specimens. In most tests, the radial displacement data during cyclic loading were somewhat noisy, and the movements were apparently of the same order as the accuracy of the measurements (±0.001 %). In reviewing the data, it was obvious that in a small number of the tests, the transducer armature had stuck initially, and these tests have been excluded.

FIG. 10 (a) *q/p'* versus radial strains for test MTRE_5 and (b) critical *q/p'* at which radial strains change significantly, plotted against relative density.

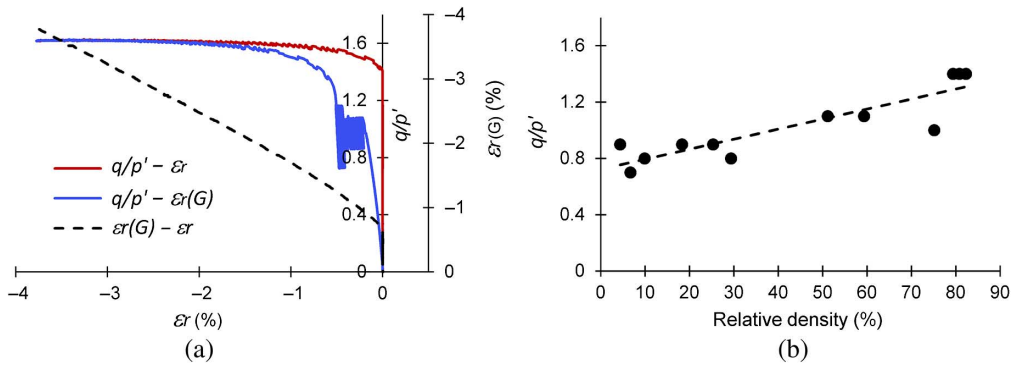

Test MTRE_6 was tested wholly in extension (see Fig. 6c), subjected to 4,000 cycles of deviatoric stress before being loaded monotonically to failure. Like the specimens tested wholly in compression, the radial strains developed during cycling were very small (0.02 % contraction).

In contrast to the aforementioned, test MTRE_1 was subjected to two stages of two-way cycling before being loaded monotonically to failure in compression (see Fig. 6e). In the first stage ($\beta = 0.32$), the specimen contracted by 0.16 % during cycling, which is significantly more than the volumetric strain observed in the tests, loaded wholly in compression or extension (tests MTRE_5 and MTRE_6, Fig. 6). In the second stage (β increased to 1.4), the accumulated radial strain reached 1.6 %. Subsequent monotonic loading resulted in a reversal of the radial strain as the specimen dilated. These differences in the radial strains directly affect the calculated volume changes, and they are the cause for the larger discrepancies between local and global determinations of volumetric strains observed in Fig. 6f.

Accumulated Volumetric Strains

A comparison between local and global accumulated volumetric strains with the number of applied cycles is presented in Fig. 11 for all the performed tests. The volumetric strains were calculated from the measurements of the local LVDTs using Eq 5, which assumes a sinusoidal shape for specimen deformation during loading. The tests in Fig. 11 have been divided in the three groups defined in Table 1 (MTRE, MTLE, and DDLE), but they have been further subdivided into loose and dense specimens depending on whether their relative density (D_r) was lower or higher than 50 %, respectively. Corroborating relevant literature (Tatsuoka and Ishihara 1974; de Groot et al. 2006), larger volumetric deformations were observed for the loose rather than dense specimens. Thus, different vertical scales have been used in the representations of Fig. 11, and this must be kept in mind when analyzing the observed experimental trends. Analysis of the results in Fig. 11, where local volumetric measurements are shown with white-filled symbols and global volumetric measurements with black-filled symbols, yielded to the following observations:

1. Common to all the groups of loose specimens (MTRE, MTLE, or DDLE), local and global volumetric trends have the same sign despite differences in magnitude (see Fig. 11a, c, and e). In contrast, for dense specimens, global and local volumetric strains can yield the opposite sign of the volumetric deformations (see Fig. 11b, d, and f). In many tests of dense specimens (e.g., MTRE5 in Fig. 11b, MTLE4 and MTLE5 in Fig. 11d, and DDLE5 in Fig. 11f), when the global volumetric measurements suggest dilation of the specimen, the local volumetric measurements indicate progressive compression.
2. For some tests (e.g., MTRE_2, MTRE_4, MTLE_1, MTLE_3, and DDLE_2, all belonging to the category of loose specimens), there are no significant disparities between local and global volumetric determination. Other tests (e.g., MTRE_1, MTRE_3, MTLE_2, and DDL5_5) exhibit similar local and global volumetric responses up to a certain value of number of cycles N (between 50 and 200), and then consistent differences can be observed. A final category of tests can be identified (e.g., MTRE_5, MTRE_6, MTLE_4, MTLE_5, DDLE_1, DDLE_3, and DDLE_4) in which the global and local volumetric strains diverge from the onset of cycling loading.
3. It is not possible to uniquely state whether global measurements overestimate or underestimate volumetric deformations if compared to the local measurements. Generally, the global volumetric determinations indicate more compression than local determinations for loose specimens cycled at low average stress levels

FIG. 11 Accumulated volumetric strains with number of cycles in logarithmic scale: (a) MTRE loose, (b) MTRE dense, (c) MTLE loose, (d) MTLE dense, (e) DDLE loose, and (f) DDLE dense.

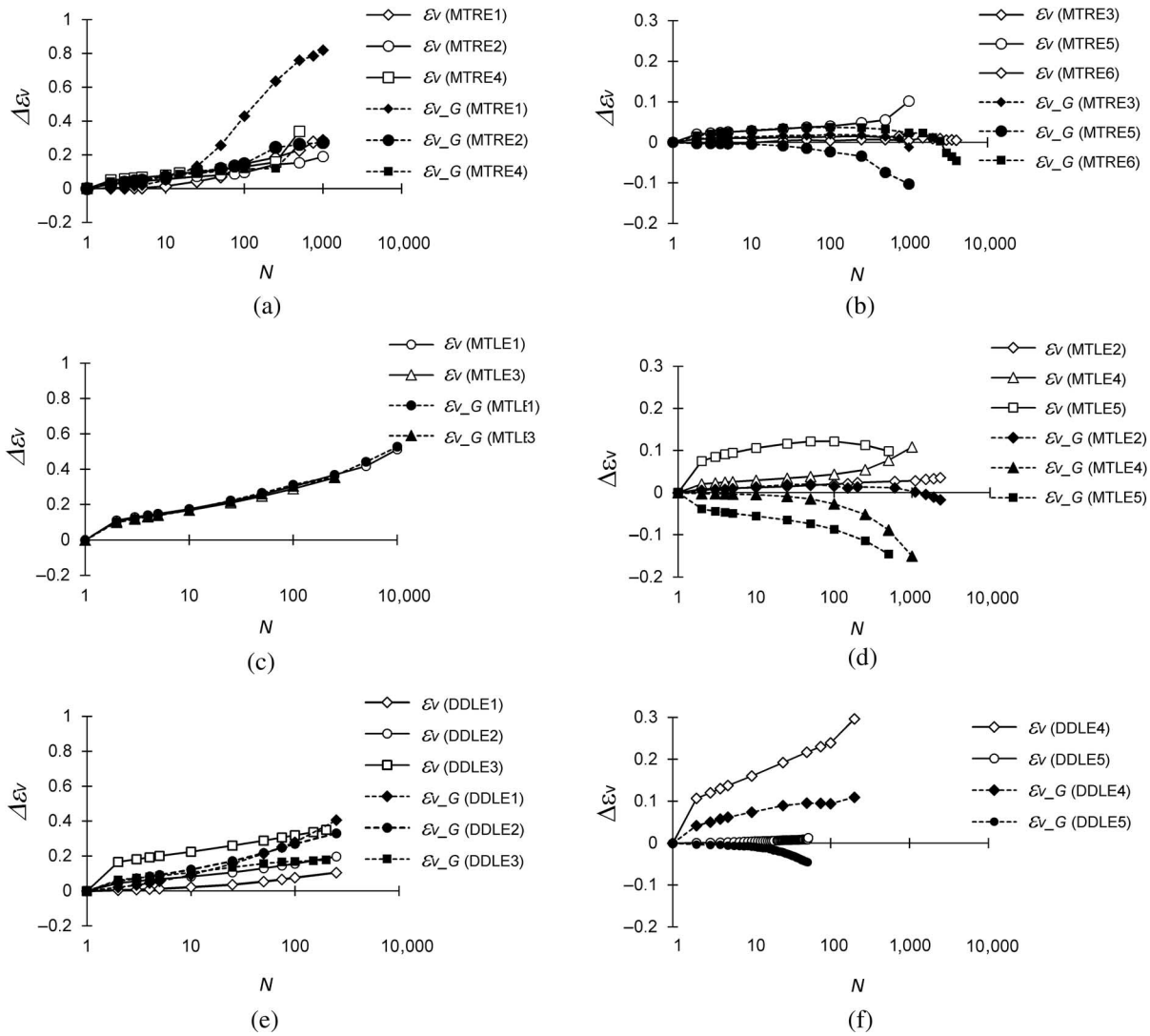

(e.g., MTRE1, DDLE1, and MTRE2 cycles at $\eta_{avg} \leq 0.25$), but less compressive or more dilative responses for all the dense specimens or other loose specimens cycled at higher average stress ratios.

The magnitude of the difference between local and global volumetric trends is also influenced by the density and stress level. For the MTRE–loose group (see Fig. 11a), the differences are more pronounced at low stress levels, while for all the dense specimens (see Fig. 11b, d, and f) the difference increases with increasing average cycling stress ratio. These differences appear to be related to the magnitude of radial strains developed in the specimens during cycling: it has been observed that larger radial strains are developed for two-way cycling at low average stress levels (see Fig. 6e) or for one-way cycling at high average stress ratios (see Fig. 10b).

FIG. 12

Cyclic number at which dense specimens diverge to negative global $\Delta\varepsilon_v$ during drained cyclic loading, against η.

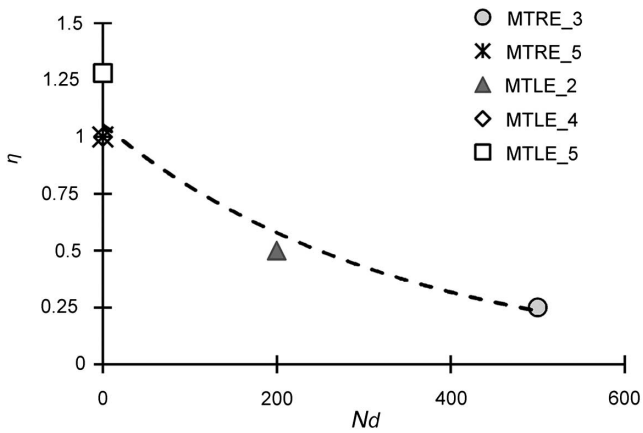

These observations suggest that the relative magnitude of the global and local volumetric deformations is affected by both relative density (D_r) and average cyclic stress ratio (η_{avg}). Indeed, it is expected that the cyclic amplitude (β) is also an important factor, but this has been kept rather constant in this experimental investigation. Fig. 12 shows how the average cyclic stress ratio affects the point during cycling (defined by the number of cycle N_d) when the dense specimens start to deform with a global volumetric strain rate of opposite sign to the locally determined volumetric strain rate. As discussed in Point 1 above, this divergence of the sign of the volumetric strain rate is rather obvious for many dense specimens, such as MTRE3, MTRE5, MTLE2, MTLE4, and MTLE5 (see Fig. 11b and d), which have been all used for drawing Fig. 12. Higher stress levels accelerate the onset of global and local measurement divergences, which can take place from the very early stage of cycling. It is worth noting that in two tests (MTLE_4 and MTLE_5 with LE), divergence was observed from the start of cycling ($N_d = 0$); these specimens were subjected to cycling at high stress ratios ($\eta_{avg} = 1.0$ and 1.25, respectively).

In order to demonstrate the differences between local and global accumulated volumetric strains and their dependence with both density and average stress ratio, the three-dimensional representations in Fig. 13 have been developed. In Fig. 13a, the values of accumulated global and local volumetric strain after 100 cycles are plotted against initial relative density (D_r) and average cyclic stress ratio (η_{avg}). Each global determination is represented by a circle, while the corresponding local determination is indicated by a triangle. The two points have been linked by a line to form an arrow which gives a visual indication of the direction and magnitude of the difference. A grid corresponding to the plane of zero volumetric strains has been included to help in understanding the figure. This representation confirms the previous observation Point 2, suggesting that global volumetric determinations overestimate compression at low average stress level and for loose specimens, but they also overestimate dilation for high stress level, dense specimens, or both. The difference between local and global determination seems to be limited for medium dense specimens' cycled at an average stress ratio of around 0.5. A clearer representation may be obtained in Fig. 13b, which used the percentage error of the volumetric determination defined as follows:

FIG. 13 (a) Plot of local (triangle end of arrow) and global (circle) volumetric strains versus relative density and average cyclic stress ratio, and (b) plot of volumetric percentage error versus relative density and average cyclic stress ratio.

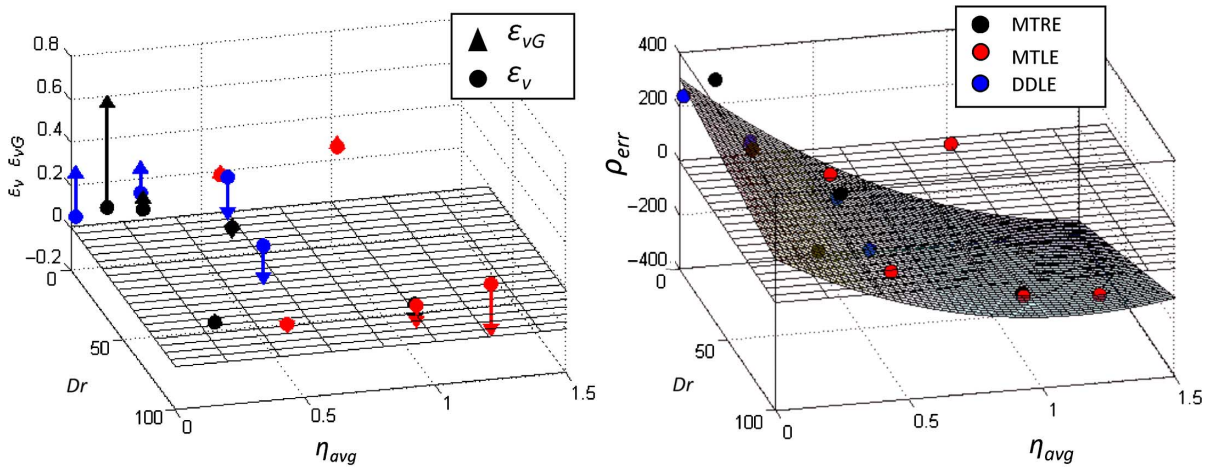

$$\rho_{err} = \frac{\Delta\varepsilon_{vG} - \Delta\varepsilon_v}{|\Delta\varepsilon_v|} \cdot 100 \tag{7}$$

With only one exception related to test MTLE3, all the points in Fig. 13 fit a second order polynomial surface quite well. This surface facilitates the understanding of the trends of volumetric error that can be recorded if external global measurements are used. A reverse of the sign of the error is observed for average stress ratio of about 0.5. It is also important to note that volumetric errors larger than 200 % can be obtained in extreme situations (e.g., very loose specimens cycled at very low stress ratios or dense specimens cycled at very high stress levels).

Discussion

The difference between the volumetric trends determined with global and local transducers highlights the degree of deformation nonuniformities that may emerge throughout a tested specimen during a monotonic and cyclic triaxial test. The difference in the sign of the global and local volumetric strains determinations observed for the dense specimens suggests that while the center of the specimen undergoes volumetric compression, as evidenced by local strain measurements, the top and bottom thirds of the specimen must experience important dilative processes to comply with the overall dilative specimen's behavior monitored by the external volume gauge. Thus, continuous cyclic loading could induce nonuniform stress states throughout the specimen, and the sole use of an external volumetric measurement system may lead to a misinterpretation of the soil response. While it may be a bit speculative, it logically follows that the consequences of these nonuniformities may be even more concerning for cyclic undrained tests. In fact, the different local tendencies for contraction or dilation between the center and the boundaries of the specimen will probably cause a differential excess pore pressure buildup throughout

the specimen, triggering water flow within the specimen, which will locally not respect the constant volume hypothesis of an undrained test. This will likely have important implications for the observed overall mechanical response.

The main parameters that will trigger the development of nonuniform deformations along the specimen are its density and the stress level. Disparities between global and local volumetric changes were observed for both loose and dense specimens, but while for loose specimens only differences in magnitude were observed, for dense specimens cycled at high stress levels the sign of the volumetric strains was often in disagreement. Larger discrepancies between local and global determinations of volumetric strains are associated with those testing conditions triggering a larger development of radial strains, which are observed for two-way cycling at low stress levels or cycling at high stress ratios. It should also be reminded that the increasing discrepancies at higher stress levels may be explained by larger shear bands or localization inside the dense specimens, which, as suggested by Desrues, Bésuelle, and Lewis (2007), are susceptible to such phenomena from the early stage of shearing.

Summary and Conclusions

Results from cyclic triaxial tests on sand specimens fabricated with two different techniques (MT and DD) and tested under both restrained and enlarged LE conditions have been analyzed to investigate the occurrence of nonuniformities of volumetric deformations and to assess the implications for the interpretation of the soil response during triaxial cyclic shearing. The occurrence of nonuniformities was assessed by comparing volumetric strain determinations from global strain measurement (using an external volume gauge), with strains determined from local axial and radial strain measurements (using local LVDTs placed on the middle third of the specimens). The following conclusions can be drawn from the test results:

- It is essential to use local strain measurements during both monotonic and cyclic loading when accurate measurements of soil deformation are needed. This should be important in the small to medium strain domain, where accurate measurements are necessary for material stiffness determination, which is essential for constitutive modeling purposes. Divergence between global and local determinations can be observed from the very beginning of the tests reported here.
- When using local instrumentation, the conventional RC assumption to determine volumetric deformation gives reliable results only for small radial deformation measured at the middle third of the specimen. In this investigation, the differences between three different assumptions for the deformed shape of the specimen (RC, parabolic, sinusoidal) became important only when the radial strain exceeded approximately −0.25 %.
- Under conditions of one-way cyclic loading, the accumulated radial strains were negligible until the stress ratio reached a critical value that varied with density. Only when cycling was two-way did significant radial strains develop.
- Comparisons between local and global volumetric determinations during cyclic triaxial loading revealed considerable discrepancies for both loose and dense specimens at different average cyclic stress levels. Larger compressive volumetric strains were indicated by global measurements in very loose specimens at low stress levels. For dense specimens cycled at high stress levels, global measurements can instead lead to a reversed sign of volumetric measurements, indicating overall

dilation, while the middle third of the specimen is contracting. These discrepancies between local and global volumetric determinations seem to be governed by the magnitude of radial strain developed during cycling, which was recorded to be larger for two-way cycling at low average stress ratios or one-way cycling at high stress ratios.

– For dense specimens, the divergence of local and global volumetric strains appeared to develop only after a certain number of cycles has been applied. The onset of this divergence appears to depend on the application of higher average cyclic stress ratios and may occur at a very early stage of cycling for very high stress ratios.
– While the use of enlarged LE, as opposed to frictional RE, may improve the overall uniformities of deformations, discrepancies between global and local determinations of volumetric strains were still observed for all the testing conditions and fabrication methods, especially for dense specimens cycled at high average stress ratios.
– Since the discrepancy between local and global volumetric determination was observed for a wide range of densities and average cyclic stress levels, the use of local instrumentation is recommended when accurate measurements of the soil response during cyclic loading are required.
– Given that nonuniform strains developed during these drained cyclic triaxial tests, even in specimens tested with enlarged LE and a height to diameter ratio of 2, it appears logical to point out that the same tendency would significantly affect the behavior during undrained cyclic triaxial tests. Differential excess pore pressures could build up within specimens, resulting in water flows within the specimen, which would then locally not respect the constant volume hypothesis of an undrained test. This would have important implications for interpreting the observed overall mechanical response of such undrained tests.

ACKNOWLEDGMENTS

We dedicate this work to Dr. David Nash, deceased June 21, 2017, our dearest colleague and friend, whose many contributions made this work possible. The first author would like to thank the geotechnical group at the University of Bristol for the technical support and infrastructure. This experimental research was carried out when the first author was a PhD student at the University of Bristol, United Kingdom. The work during the final process of this article has been supported by CONICYT PAI/ACADEMIA 79150011.

Appendix: Derivation of Formulas for Volumetric Strain

PARABOLIC EXPRESSION FOR LOCAL VOLUMETRIC STRAIN

Assuming a parabolic variation of diameter, we use the following:

$$D = D_1 - (D_1 - D_0)\left(\frac{2y}{H}\right)^2 \tag{A1}$$

Where D_1 is the diameter at mid-height $y/H = 0$, D_0 is the diameter at the ends $2y/H = 1$ (see Fig. 1), and $2y$ corresponds to the total gauge length L.

The average diameter over length $+y$ to $-y$ can be obtained from the following:

$$\text{Volume } V = \int_{-y}^{y} \frac{\pi}{4} D^2 dy \tag{A2}$$

$$D^2 = D_1^2 - 2D_1(D_1 - D_0)\left(\frac{2y}{H}\right)^2 + (D_1 - D_0)^2\left(\frac{2y}{H}\right)^4 \tag{A3}$$

So, for a given value of H, we have the following:

$$V = \frac{\pi}{2}\left[D_1^2 - \frac{2}{3}D_1(D_1 - D_0)\left(\frac{2y}{H}\right)^2 + \frac{1}{5}(D_1 - D_0)^2\left(\frac{2y}{H}\right)^4\right]y \tag{A4}$$

During a test, L and H vary, but we assume L/H remains constant:

$$V = \frac{\pi}{2}\left[D_1^2 - \frac{2}{3}D_1(D_1 - D_0)\left(\frac{L}{H}\right)^2 + \frac{1}{5}(D_1 - D_0)^2\left(\frac{L}{H}\right)^4\right]y \tag{A5}$$

The changing diameter at mid-height D_1 is measured by the radial strain transducer, and the changing gauge length L is measured by the axial local strain transducers.

$$\text{Writing:} \quad \Delta y = y - y_0; \quad \Delta D = D_1 - D_0 \tag{A6}$$

Hence, we have the following:

$$V = \frac{\pi}{2}\left[(D_0 + \Delta D)^2 - \frac{2}{3}(D_0 + \Delta D)(\Delta D)\left(\frac{L}{H}\right)^2 + \frac{1}{5}(\Delta D)^2\left(\frac{L}{H}\right)^4\right](y_0 + \Delta y) \tag{A7}$$

The average area $A = V/L$ and the average diameter $\overline{D} = \sqrt{\frac{4A}{\pi}}$

$$\text{As} \quad V_0 = \frac{\pi}{2}D_0{}^2 y_0 \ \textit{and}\ \Delta V = V - V_0 \tag{A8}$$

$$\Delta \mathrm{V} = \frac{\pi}{2}\left[\left(2\mathrm{D}_0\Delta\mathrm{D}\left(1 - \frac{1}{3}\left(\frac{L}{H}\right)^2\right) + \Delta\mathrm{D}^2\left(1 - \frac{2}{3}\left(\frac{L}{H}\right)^2 + \frac{1}{5}\left(\frac{L}{H}\right)^4\right)\right)(\mathrm{y}_0 - \Delta\mathrm{y}) + \mathrm{D}_0^2\Delta\mathrm{y}\right] \tag{A9}$$

Eq A9 can now be divided by V_0 to give the following:

$$\frac{\Delta \mathrm{V}}{\mathrm{V}_0} = \left[2\left(1 - \frac{1}{3}\left(\frac{L}{H}\right)^2\right)\frac{\Delta\mathrm{D}}{\mathrm{D}_0} + \left(-1 + \frac{2}{3}\left(\frac{L}{H}\right)^2 - \frac{1}{5}\left(\frac{L}{H}\right)^4\right)\frac{\Delta\mathrm{D}^2}{\mathrm{D}_0^2}\right]\left(1 - \frac{\Delta\mathrm{y}}{y_0}\right) + \frac{\Delta\mathrm{y}}{\mathrm{y}_0} \tag{A10}$$

and introducing the expression for volumetric strains ($\varepsilon_v = -\Delta V/V_0$), axial strains ($\varepsilon_a = -\Delta y/y_0$) and radial strains ($\varepsilon_r = -\Delta D/D_0$), it is possible to obtain the following:

$$\varepsilon_\mathrm{v} = \left[2\left(1 - \frac{1}{3}\left(\frac{L}{H}\right)^2\right)\varepsilon_\mathrm{r} + \left(-1 + \frac{2}{3}\left(\frac{L}{H}\right)^2 - \frac{1}{5}\left(\frac{L}{H}\right)^4\right)\varepsilon_\mathrm{r}^2\right](1 - \varepsilon_\mathrm{a}) + \varepsilon_\mathrm{a} \tag{A11}$$

SINUSOIDAL EXPRESSION FOR LOCAL VOLUMETRIC STRAIN

Assuming a sinusoidal variation of diameter, we use the following:

$$D = D_0 - \frac{\Delta D}{2}\left(1 + cos\left(\frac{2\pi y}{H}\right)\right) \tag{A12}$$

Where $D_0 + \Delta D$ is the diameter at mid-height $2y/H = 0$, and D_0 is the diameter at the ends, $2y/H = 1$ (see Fig. 1).

The average diameter over length +y to −y can be obtained from the following:

$$\text{Volume } V = \int_{-y}^{y} \frac{\pi}{4} D^2 dy \tag{A13}$$

$$D^2 = D_0^2 - D_0 \cdot \Delta D \cdot \left(1 + cos\left(\frac{2\pi y}{H}\right)\right) + \frac{\Delta D^2}{4}\left(1 + 2cos\left(\frac{2\pi y}{H}\right) + cos^2\left(\frac{2\pi y}{H}\right)\right) \tag{A14}$$

So for a given value of H, we have the following:

$$V = \frac{\pi}{2}\left[D_0^2 - D_0.\Delta D + \frac{3}{8}\Delta D^2 + \frac{\Delta D}{\pi\left(\frac{2y}{H}\right)}\left(-D_0 + \frac{\Delta D}{2}\right) sin\left(\frac{2\pi y}{H}\right) + \frac{\Delta D^2}{16\pi\left(\frac{2y}{H}\right)} sin\left(\frac{4\pi y}{H}\right)\right] y \tag{A15}$$

During a test, L and H vary, but we assume $L/H =$ remains constant:

$$V = \frac{\pi}{2}\left[D_0^2 - D_0.\Delta D + \frac{3}{8}\Delta D^2 + \frac{\Delta D}{\pi\frac{L}{H}}\left(-D_0 + \frac{\Delta D}{2}\right) sin\left(\pi\frac{L}{H}\right) + \frac{\Delta D^2}{16\pi\frac{L}{H}} sin\left(2\pi\frac{L}{H}\right)\right] y \tag{A16}$$

The changing diameter at mid-height D_1 is measured by the radial strain transducer, and the changing gauge length y is measured by the axial local strain transducers.

$$\text{Writing} \quad \Delta y = y - y_0; \quad \Delta D = D_1 - D_0 \tag{A17}$$

$$V = \frac{\pi}{2}\left[D_0^2 + D_0.\Delta D + \frac{3}{8}\Delta D^2 + \frac{\Delta D}{\pi\left(\frac{L}{H}\right)}\left(-D_0 + \frac{\Delta D}{2}\right) sin\left(\frac{\pi L}{H}\right) + \frac{\Delta D^2}{16\pi(L/H)} sin\left(\frac{2\pi L}{H}\right)\right](y_0 - \Delta y) \tag{A18}$$

The average area $A = V/L$, and the average diameter $\overline{D} = \sqrt{\frac{4A}{\pi}}$

$$\text{As } V_0 = \frac{\pi}{2} D_0{}^2 y_0 \text{ and } \Delta V = V_o - V \tag{A19}$$

$$\Delta V = \frac{\pi}{2}\left[\left(D_0 \cdot \Delta D - \frac{3}{8}\Delta D^2 - \frac{\Delta D}{\pi\left(\frac{L}{H}\right)}\left(-D_0 + \frac{\Delta D}{2}\right) sin\left(\pi\frac{L}{H}\right) - \frac{\Delta D^2}{16\pi(L/H)} sin\left(2\pi\frac{L}{H}\right)\right)(y_0 - \Delta y) + D_0^2 \Delta y\right] \tag{A20}$$

Expressing this as strains by dividing by V_0, it is possible to obtain a final relationship:

$$\frac{\Delta V}{V_0} = \left[\left(1 + \frac{1}{\pi(L/H)} sin\left(\pi\frac{L}{H}\right)\right)\frac{\Delta D}{D_0} + \left(-\frac{3}{8} - \frac{sin\left(\frac{\pi L}{H}\right)}{2\pi\left(\frac{L}{H}\right)} - \frac{sin(2\pi L/H)}{16\pi(L/H)}\right)\frac{\Delta D^2}{D_0^2}\right]\left(1 - \frac{\Delta y}{y_0}\right) + \frac{\Delta y}{y_0} \tag{A21}$$

$$\varepsilon_{vol} = \left[\left(1 + \frac{H}{\pi L} sin\left(\pi\frac{L}{H}\right)\right)\varepsilon_r + \left(-\frac{3}{8} - \frac{sin\left(\frac{\pi L}{H}\right)}{2\pi\left(\frac{L}{H}\right)} - \frac{1}{16}\frac{sin(2\pi L/H)}{\pi(L/H)}\right)\varepsilon_r^2\right](1 - \varepsilon_a) + \varepsilon_a \tag{A22}$$

References

Bishop, A. W. and Green, G. E., 1965, "The Influence of End Restraint on the Compression Strength of a Cohesionless Soil," *Géotechnique*, Vol. 15, No. 3, pp. 243–266, https://doi.org/10.1680/geot.1965.15.3.243

Bishop, A. W. and Wesley, L. D., 1975, "A Hydraulic Triaxial Apparatus for Controlled Stress Path Testing," *Géotechnique*, Vol. 25, No. 4, pp. 657–670.

Colliat-Dangus, J. L., Desrues, J., and Foray, P., 1988, "Triaxial Testing of Granular Soil under Elevated Cell Pressure," *Advanced Triaxial Testing of Soil and Rock, ASTM STP977*, ASTM International, West Conshohocken, PA, 900p., https://doi.org/10.1520/STP29082S

Corti, R., Diambra, A., Wood, D. M., Escribano, D. E., and Nash, D. F., 2016, "Memory Surface Hardening Model for Granular Soils under Repeated Loading Conditions," *J. Eng. Mech.*, Vol. 142, No. 12, 04016102, https://doi.org/10.1061/(ASCE)EM.1943-7889.0001174

Cuccovillo, T. and Coop, M. R., 1997, "The Measurement of Local Axial Strains in Triaxial Tests Using LVDTs," *Géotechnique*, Vol. 47, No. 1, pp. 167–171, https://doi.org/10.1680/geot.1997.47.1.167

Desrues, J., 1990, "Shear Band Initiation in Granular Materials: Experimentation and Theory," *Geomaterials: Constitutive Equations and Modelling*, CRC Press, Boca Raton, FL, pp. 283–310.

Desrues, J., 1984, "La Localisation de la Deformation dans les Materiaux Granulaires," Ph.D. dissertation, Université Scientifique et Medicale de Grnoble, Grenoble, France.

Desrues, J., Bésuelle, P., and Lewis, H., 2007, "Strain Localization in Geomaterials," *Geol. Soc., London*, Vol. 289, pp. 47–73, https://doi.org/10.1144/SP289.4

Diambra, A., Ibraim, E., Russell, A. R., and Muir Wood, D., 2011, "Modelling the Undrained Response of Fiber Reinforced Sands," *Soils Found.*, Vol. 51, No. 4, pp. 625–636, https://doi.org/10.3208/sandf.51.625

Doanh, T. and Ibraim, E., 2000, "Minimum Undrained Strength of Hostun RF Sand," *Géotechnique*, Vol. 50, No. 4, pp. 377–392, https://doi.org/10.1680/geot.2000.50.4.377

Escribano, D. E., 2014, "Evolution of Stiffness and Deformation of Hostun Sand under Drained Cyclic Loading," Ph.D. thesis, University of Bristol, Bristol, United Kingdom.

Flavigny, E., Desrues, J., and Palayer, B., 1990, "Le Sable d'Hostun RF," *Rev. Fr. Géotech.*, Vol. 53, pp. 67–70, https://doi.org/10.1051/geotech/1990053067

Germaine, J. T. and Ladd, C. C., 1988, "Triaxial Testing of Saturated Cohesive Soils," *Advanced Triaxial Testing for Soil and Rock, ASTM STP977*, ASTM International, West Conshohocken, PA, pp. 421–459, https://doi.org/10.1520/STP29091S

Goto, S. and Tatsuoka, F., 1988, "Effects of End Conditions on Triaxial Compressive Strength for Cohesionless Soil," *Advanced Triaxial Testing of Soil and Rock, ASTM STP977*, ASTM International, West Conshohocken, PA, pp. 692–705, https://doi.org/10.1520/STP29108S

de Groot, M. B., Bolton, M. D., Foray, P., Meijers, P., Palmer, A. C., Sandven, R., Sawicki, A., and Teh, T. C., 2006, "Physics of Liquefaction Phenomena around Marine Structures," *J. Waterw. Port Coastal Ocean Eng.*, Vol. 132, No. 4, pp. 227–243.

Ibraim, E. and Fourmont, S., 2006, "Behaviour of Sand Reinforced with Fibres," *Soil Stress-Strain Behaviour: Measurement, Modelling and Analysis*, Springer, Berlin, Germany, pp. 807–818.

Ishihara, K., 1993, "Liquefaction and Flow Failure during Earthquakes," *Géotechnique*, Vol. 43, No. 3, pp. 349–451, https://doi.org/10.1680/geot.1993.43.3.351

Kirkpatrick, W. M. and Belshaw, D. J., 1968, "On the Interpretation of the Triaxial Test," *Géotechnique*, Vol. 18, No. 3, pp. 336–350, https://doi.org/10.1680/geot.1968.18.3.336

Klotz, E. U. and Coop, M. R., 2002, "On the Identification of Critical State Lines for Sands," *Geotech. Test. J.*, Vol. 25, No. 3, pp. 288–301, https://doi.org/10.1520/GTJ11090J

Ladd, R. S., 1978, "Preparing Test Specimens Using Undercompaction," *Geotech. Test. J.*, Vol. 1, No. 1, pp. 16–23, https://doi.org/10.1520/GTJ10364J

Linton, P. F., McVay, M. C., and Bloomquist, D., 1988, "Measurement of Deformation in the Standard Triaxial Environment with a Comparison of Local versus Global Measurements

on a Fine, Fully Drained Sand," *Advanced Triaxial Testing of Soil and Rock, ASTM STP977*, ASTM International, West Conshohocken, PA, pp. 202–215, https://doi.org/10.1520/STP29079S

Liu, X., Longtan, S., and Xiaoxia, G., 2013, "Local Data Analysis for Eliminating End Restraint of Triaxial Specimen," *Trans. Tianjin Univ.*, Vol. 19, No. 5, pp. 372–380, https://doi.org/10.1007/s12209-013-2000-1

Rowe, P. W. and Barden, L., 1964, "The Importance of Free-Ends in the Triaxial Test," *J. Soil Mech. Found. Div.*, Vol. 90, No. 1, pp. 1–27.

Sadek, T., 2006, "The Multiaxial Behaviour and Elastic Stiffness of Hostun Sand," Ph.D. thesis, University of Bristol, Bristol, United Kingdom.

Tatsuoka, F. and Ishihara, K., 1974, "Yielding of Sand in Triaxial Compression," *Soils Found.*, Vol. 14, No. 2, pp. 63–76, https://doi.org/10.3208/sandf1972.14.2_63

Vardoulakis, I. and Drescher, A., 1985, "Behaviour of Granular Soil Specimens in the Triaxial Compression Test," *Developments in Soil Mechanics and Foundation Engineering, Vol. 2*, Elsevier, Amsterdam, the Netherlands, pp. 215–252.

Zhang, H. and Garga, V. K., 1997, "Quasi-Steady State: A Real Behaviour?" *Can. Geotech. J.*, Vol. 34, No. 5, pp. 749–761, https://doi.org/10.1139/t97-046